ELSEVIER

Journal of Alloys and Compounds 234 (1996) 67–82

Journal of ALLOYS AND COMPOUNDS

Amorphization process by rod-milling Ti_xAl_{100-x} and the effect of annealing

M. Sherif El-Eskandarany[1]

Mining and Petroleum Engineering Department, Faculty of Engineering, Al-Azhar University, 11884-Nasr City, Cairo, Egypt

Received 8 May 1995

Abstract

Amorphous Ti_xAl_{100-x} alloy powders with wide amorphization range ($33 \leq x \leq 75$) have been synthesized by rod-milling technique using a mechanical alloying (MA) process. The rod-milled alloy powders have been investigated by means of X-ray diffraction, differential scanning calorimetry, optical microscopy, scanning electron microscopy and transmission electron microscopy. The results have shown that during the first few kiloseconds (11–360 ks) of the mechanical deformation via the rod-milling technique, the layered composite particles of Ti and Al are intermixed and form an amorphous phase when heated at about 700 K by so-called thermally assisted solid state amorphization (TASSA). The heat formation of an amorphous (enthalpy change of amorphization) Ti_xAl_{100-x} alloy via the TASSA process, ΔH_a^{TASSA}, has been measured directly as a function of the MA time. The crystallization characteristics indexed by the crystallization temperature T_x^{TASSA} and the enthalpy change of crystallization, ΔH_x^{TASSA}, of the amorphous phase formed via the TASSA process are also investigated as a function of the MA time. Comparable with the TASSA process, a homogeneous amorphous of Ti_xAl_{100-x} alloy has been formed directly without heating the composite particles after a longer MA time (1400 ks). The amorphization process in this case is attributed to a mechanical driven solid state amorphization (MDSSA). At the end of the MA processing time (360–1440 ks), the maximum heat formation of an amorphous Ti_xAl_{100-x} alloy via the MDSSA process ΔH_a^{MDSSA} has been estimated. Moreover, the thermal stability characterized by the crystallization temperature, T_x^{MDSSA}, and the enthalpy change of crystallization, ΔH_x^{MDSSA}, are also presented. The role of amorphization of Ti_xAl_{100-x} alloy powders for each process has been discussed.

Keywords: Amorphous Ti–Al alloys; Mechanical alloying; Crystallization

1. Introduction

The term ball-milling may be referred to as the process of breaking down the relatively coarse material to the ultimate fineness. The purposes for which solids are comminuted have been to decrease the size of material, to increase the surface area of material and/or to free material from its matrices. This process has been used via tumbling mills or vibration mills for comminution of ores, preparing materials for industrial applications, such as grinding of talc to prepare body powder, grinding of iron ore for preparation of pellets and many others.

Apart from the grinding of ores, and the separation of the useful constituents of minerals for their subsequent beneficiation, Koch employed a high energy ball-mill for producing homogeneous amorphous alloy starting from two elemental metals (Ni and Nb powders) by the so-called mechanical alloying (MA) process [1]. Since then, ball-milling [2–14] and/or rod-milling [15–29] techniques have been successfully employed via MA for formation of several metallic amorphous alloys and compounds, including metal silicides, metal nitrides and metal carbides [30–45]. More recently, the MA process has been employed for reducing several metal oxides by milling the oxide materials with metallic reducing agents using a method so-called mechanical solid state reduction (MSSR) [46–48].

In this work, the rod-milling technique has been used for preparation of composite powder particles containing mechanically-deformed multilayers of elemental Ti and Al powders. The choice of this type of mill comes from the fact that this is the most suitable mill for the effective application of shear force

[1] Present address: Institute for Materials Research, Tohoku University, Katahira 2-1-1, Sendai 980-77, Japan.

SSDI 0925-8388(95)01947-2

for formation of uniform well-arranged numerous layered composite particles via the MA method [15,29]. The influence of so-called thermally assisted solid state amorphization (TASSA) [18] on the behavior and structure of these multilayered particles has been presented. Moreover, the progress of glass formation of Ti_xAl_{100-x} alloy powders directly formed due to mechanically driven solid state amorphization (MDSSA) via the MA technique has also been studied. For the purpose of the present work, X-ray diffraction (XRD), differential scanning calorimetry (DSC), optical microscopy, scanning electron microscopy (SEM), and transmission electron microscopy (TEM) has been utilized to monitor the crystal-to-amorphous phase transition in Ti_xAl_{100-x} alloy powders. The present work aims to clarify the mechanism of the amorphization process by way of TASSA and MDSSA during MA of elemental Ti and Al powders in a rod-mill.

2. Experimental details

Pure elemental powders of Ti and Al (50 μm, 99.99%) were mixed to give the desired average composition of Ti_xAl_{100-x} in a glove box under a purified argon atmosphere (O_2 and H_2O less than 1 ppm) and sealed in a cylindrical stainless steel shell (SUS 304, 120 mm in diameter) together with ten stainless steel rods (SUS 304, 10 mm in diameter) [15]. The rod-to-powder weight ratio was controlled to be about 30:1. The dry rod-milling was carried out at ambient temperature by mounting the rod-mill on a rotator at the rate of 1.4 s^{-1} [21,42]. The MA experiments were interrupted at regular intervals and a small amount of the rod-milled powder was taken out from the vial in the glove box. The structure and the amorphization progress of the rod-milled powders have been characterized by means of XRD with Cu Kα, and DSC under an argon gas flow. All the DSC results presented in this study were obtained with heating rates of 0.67 K s^{-1}. However, some alloys have been heated at several different heating rates (0.042, 0.083, 0.167, 0.333, 0.500, and 0.833 K s^{-1}) to determine the activation energies of amorphization E_a using the Kissinger method [49]. The morphology of the alloyed powders was studied by SEM-electron probe microanalyses (EPMA), using a 30 kV microscope and TEM using a 200 kV microscope. However, high resolution transmission electron microscopy (HRTEM) using a 1 MV microscope, has been used for the characterization of some mechanically alloyed powders. All the samples for TEM observations were prepared by mixing the powders with ethanol and mounting the suspended powders on a copper microgrid [16,44]. Moreover, the induction coupled plasma (ICP) emission method was used to analyze the contents of Ti and Al, and the degree of Fe contamination in the milled powder. The oxygen in the alloy powders was determined by the helium carrier fusion–thermal conductivity method. The end-product of Ti_xAl_{100-x} alloy powders contain less than 0.25 at.% and 0.70 at.% contamination by iron and oxygen respectively.

3. Results

3.1. Structural change with the milling time

3.1.1. X-ray analysis

The total change in structure of rod-milled Ti_xAl_{100-x} alloy powders during the progress of MA has been investigated by X-ray analyses. The XRD patterns of the end-product (1440 ks of MA time) of Ti_xAl_{100-x} powders are presented in Fig. 1 as a function of the atomic percent of Ti content x. Obviously, the amorphous-forming range is wide, extending from 33–75 at.% Ti.

In order to understand the effect of the MA time on the total structure of Ti_xAl_{100-x} powders, samples were taken after selected milling times for X-ray analyses. Fig. 2 presents the correlation between MA time and the powder's structural changes, taking $Ti_{50}Al_{50}$ alloy as a typical example. The XRD patterns of the powders at the initial stage of MA (0 ks) reveal sharp Bragg-peaks corresponding to h.c.p.-Ti and f.c.c.-Al crystals, as shown in Fig. 2(a). Between the early stage of milling and after 173 ks of MA time (Fig. 2(b)) the Bragg-peaks for Ti and Al reflections become wider and their intensities are drastically decreased. It is worth noting that at this stage of milling, there is no evidence for the formation of any amorphous phases.

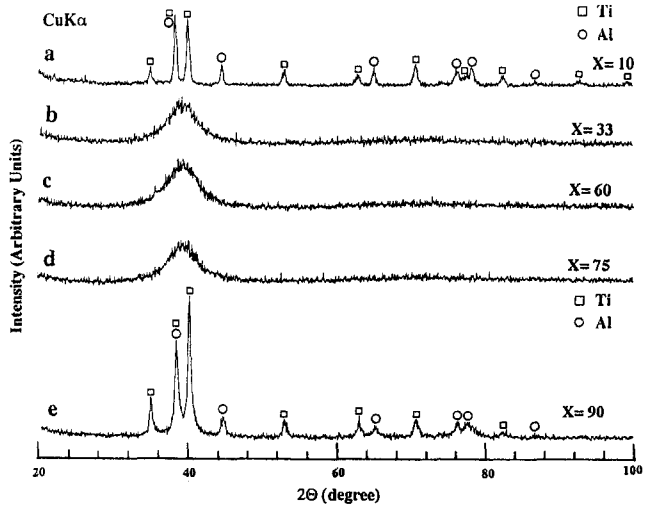

Fig. 1. XRD patterns of rod-milled Ti_xAl_{100-x} powders after 1440 ks of MA time.

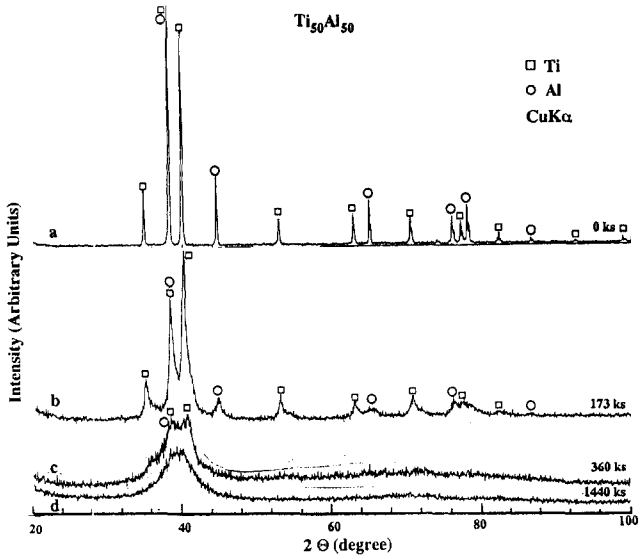

Fig. 2. XRD patterns of rod-milled $Ti_{50}Al_{50}$ powders after selected MA processing times.

During the next stage of milling (360 ks) these peaks become broader with clear diffuse haloes, suggesting the formation of an amorphous phase coexisting with Ti and Al crystals, as illustrated in Fig. 2(c). At the final stage of rod-milling (1440 ks) a homogeneous amorphous phase is yielded, characterized by diffuse haloes and smooth peaks, as shown in Fig. 2(d).

3.1.2. TEM observations

TEM analyses have been used to understand and recognize the local structure, including the heterogeneity and homogeneity of the powders during the different stages of MA. Fig. 3(a) presents the bright-field image (BFI) and Fig. 3(b) the selected-area diffraction pattern (SADP) for rod-milled $Ti_{50}Al_{50}$ powder particles after 11 ks of milling. Numerous faults with grain boundary fringes and heavy dislocations in the boundary appear clearly in the powders as a result of the shear stress generated by the milling media (rods) [15,42,44], as shown in Fig. 3(a). The corresponding SADP suggests the existence of large cells of polycrystalline Ti and Al grains, characterized by the sharp spot patterns (Laue spots) that are shown in Fig. 3(b).

The HRTEM micrograph of $Ti_{50}Al_{50}$ powders taken after 256 ks of MA time is shown, together with the corresponding SADPs, in Fig. 4. Significant heterogeneity in the local structure of the powders can be distinguished (Fig. 4(a)). According to this variety in the local structure, three different morphological regions (I, II and III) are chosen as SADPs and presented in Figs. 4(b), 4(c) and 4(d) respectively. In regions I and II, the oriented particle has twin and nanotwin boundaries on unprocessed Ti (region I) and Al (region II) particles, suggested by the spot rings shown in Figs. 4(b) and 4(c) respectively. Moreover, several defects with grain boundary movement are clearly visible near the center and at the lower and upper edges of the micrographs (Fig. 4(a)). Contrary to this, a fine structure is observed at the right upper edge of the particle (region III) presented in Fig. 4(a). The SADP show a clear halo pattern, indicating the existence of an amorphous phase in the milled powders, as shown in Fig. 4(d).

Fig. 5 shows the HRTEM image and the corresponding SADP for $Ti_{50}Al_{50}$ powders taken after 360 ks of MA time. Obviously, the sample has a rather fine structure matrix containing some twins and nanotwins with fringe images of h.c.p.-Ti and f.c.c.-Al crystals. The SADP exhibits the halo pattern of amorphous $Ti_{50}Al_{50}$ alloy overlapped with Ti and Al, as shown in Fig. 5.

The BFI and the corresponding SADP of the end-product $Ti_{50}Al_{50}$ powders (1440 ks), are shown together in Fig. 6. Overall, the sample appears to have a homogeneous fine structure with no dominant facet structure (Fig. 6(a)). Moreover, the SADP (Fig. 6(b)) shows a typical halo pattern of an amorphous phase, in good agreement with the XRD patterns presented in Fig. 2.

3.2. Morphology and metallography changes with milling time

Detailed SEM observations were performed to determine the topology and the particle size of the powders during the different stages of the MA process. Fig. 7 displays the SEM micrographs of rod-milled $Ti_{50}Al_{50}$ alloy powders after selected MA times. At the starting stage of milling (0 ks), the powders contain a mixture of random size elemental Ti and Al with block-like morphology, as shown in Fig. 7(a). After a few kiloseconds of milling (43 ks) the particles become larger (about 600 μm or more in diameter), having globe shape with cabbage leaf-like morphology [20], as shown in Fig. 7(b). The optical metallographic examinations of the cross-section for the polished and etched particles show that the powder particles contain many irregular layers of Ti and Al (Fig. 8(a)). Further milling (173 ks) enhances the shear forces generated by the rods, leading to the formation of composite powder particles containing several thin layers of Ti and Al in regular arrangement; each individual layer has a width of about 5 μm or less, as illustrated in Fig. 8(b). In addition, the reaction zones or so-called interfaces between the fresh layers of Ti and Al are increased. During this stage, a dramatic disintegration in the agglomerated powder particles take place so that the size of the individual particle decreases sharply to be in the range of 10 to 30 μm in diameter, as presented in Fig. 7(c).

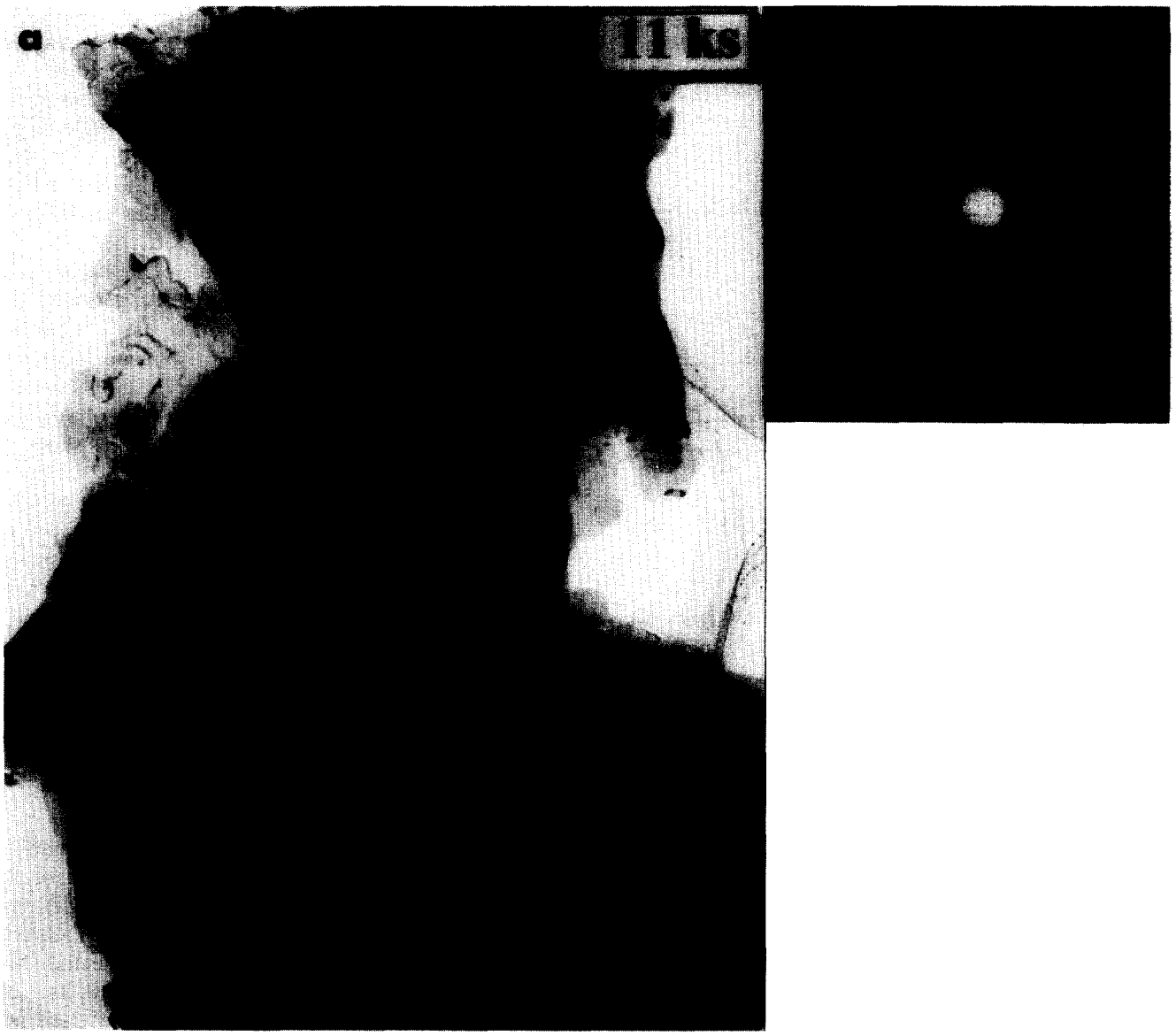

Fig. 3. BFI and SADP taken from a sample of rod-milled $Ti_{50}Al_{50}$ powders after 11 ks of MA time.

Fig. 9 shows the X-ray maps of elemental Ti (a) and Al (b) for 173 ks alloy powders. Obviously, the microstructure of the sample is layered, suggested by segregation of the elements in a composite particle on a micron scale, as shown in Figs. 9(a) and 9(b). After 360 ks of MA time, the optical metallography of the cross-sectional view for the powder particles shows that the elemental layers of Ti and Al become indistinct (Fig. 8(c)), suggesting the completion of the solid state reaction. Towards the end of MA (1440 ks), the elemental diffusion couples of Ti and Al are distributed uniformly, indicating the formation of a single homogeneous phase, as displayed in Fig. 10. Moreover, the powder particles of the end product become uniform in size (less than 3 μm in diameter) and have an almost spherical morphology, as shown in Fig. 7(d).

Figs. 11 and 12 summarize the SEM and metallographic observations of rod-milled $Ti_{50}Al_{50}$ alloy powders at the different stages of milling. Obviously, the MA process performed by the rod-milling technique can be classified into three stages: early or agglomeration; intermediate or disintegration; final or homogenization. At the agglomeration stage (0–43 ks) the alloying elemental powders of Ti and Al are agglomerated and grow in size as a result of the repeated cold welding. During this stage of milling, the powders vary widely in size from 150 to about 680 μm (Fig. 11); this is accompanied by an increment in the layer thickness and the number of layers for the individual particles, as shown in Fig. 12. During the subsequent disintegration stage (43–360 ks), the agglomerated powder particles are subjected to a continuous disintegration with fragmentation to form finer powders with size less than 20 μm in diameter. This stage of milling provides

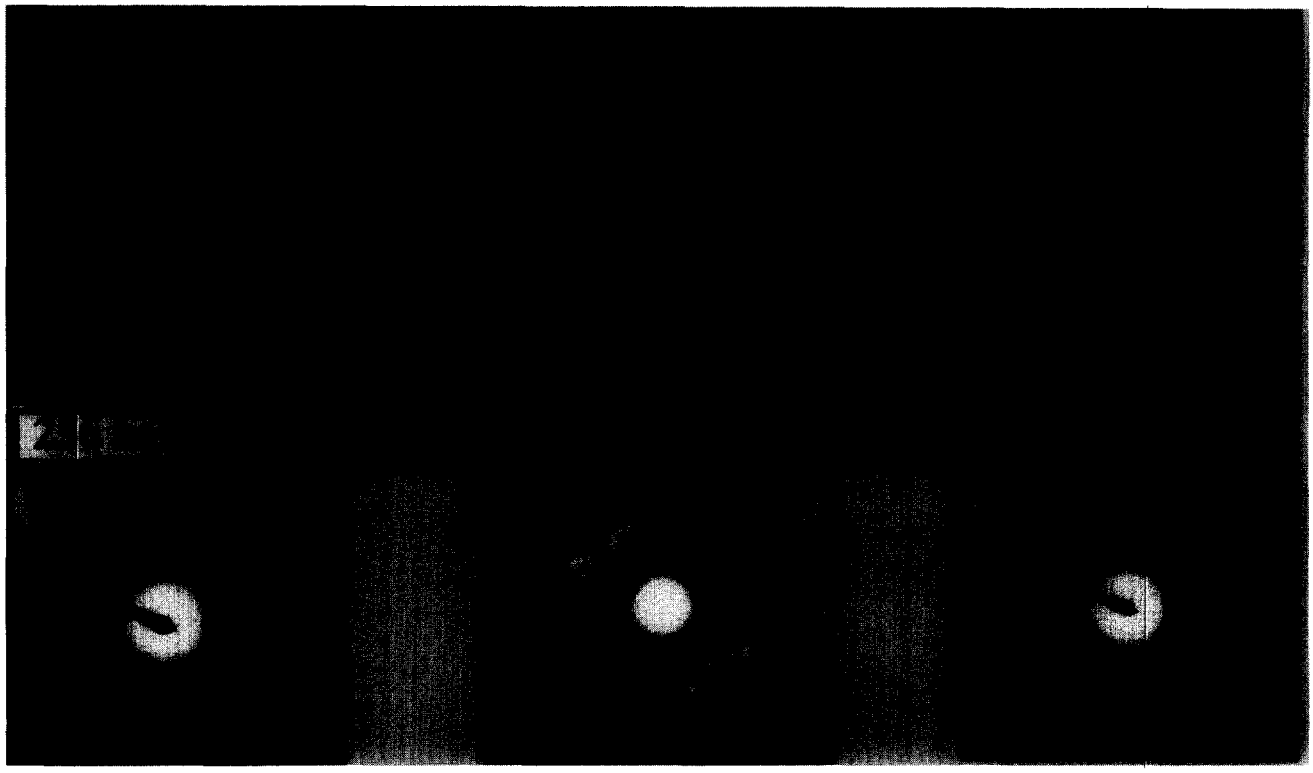

Fig. 4. HRTEM image (a) and corresponding electron diffraction patterns of three selected zones (b, c and d) taken from a sample of rod-milled $Ti_{50}Al_{50}$ powders after 256 ks of MA time.

very fine Ti–Al composite powder particles with narrow size distribution, as shown in Fig. 11. Furthermore, the layer thickness of the particles is dramatically decreased, as displayed in Fig. 12. The final or so-called homogenization stage (360–1440 ks) refers to the last stage of MA in which all the particles are uniform in shape and size and without any metallographical details. The end product of this stage is ultra fine amorphous powders.

3.3. Thermal stability

3.3.1. Amorphization process

The typical DSC thermograph of rod-milled $Ti_{50}Al_{50}$ alloy powders is presented in Fig. 13 as a function of the MA time. The measurements were made at a constant heating rate of 0.67 K s^{-1} under flow of argon gas. All the samples were heated up to 1000 K (first run) and cooled down to about 400 K. Then, second heating runs (dashed lines) were performed in order to establish the base line. Remarkably, after 11 ks there are two reactions. The first reaction, observed at about 930 K, is endothermic and is due to the melting of pure Al in the starting material of $Ti_{50}Al_{50}$ powders. The second reaction (exothermic) occurs at about 965 K and is attributed to a partial reaction of the unprocessed materials of Ti and Al powders. After 43 ks of milling, however, the endothermic and exothermic reaction peaks have already disappeared and the scan reveals two separate exothermic reactions. The peak temperature of the first exothermic peak does not change with the progress of the MA time and is situated at around 625 K, as shown in Fig. 13. Hence, the activation energy of amorphization E_a (determined by the Kissinger method [49]) is substantially independent of the MA time, as shown in Table 1. Contrary to this, the peak temperature of the second exothermic peak is shifted to elevated temperature during the early and intermediate stages of milling. At the final stage of milling, the second exothermic peak becomes pronounced and sharp, while the first exothermic peak surprisingly disappears. It is worth noting that when the starting material was an intermetallic TiAl powder, i.e. a mechanical disordering (MD) process, the first exothermic reaction is absent [50]. The same observation was noticed for other compositions of rod-milled Ti_xAl_{100-x} powders [51]. In order to identify the origin of these exothermic reactions, three samples of 173 ks mechanically alloyed powders were heated separately in the DSC for TEM investigations at points (a), (b) and (c) in Fig. 13. The TEM observations allowed direct imaging of the phase formed for each reaction. The BFIs and the corresponding SADPs of the samples heated up to 410 K (far below the first reaction), 700 K (just above the first reaction), and 980

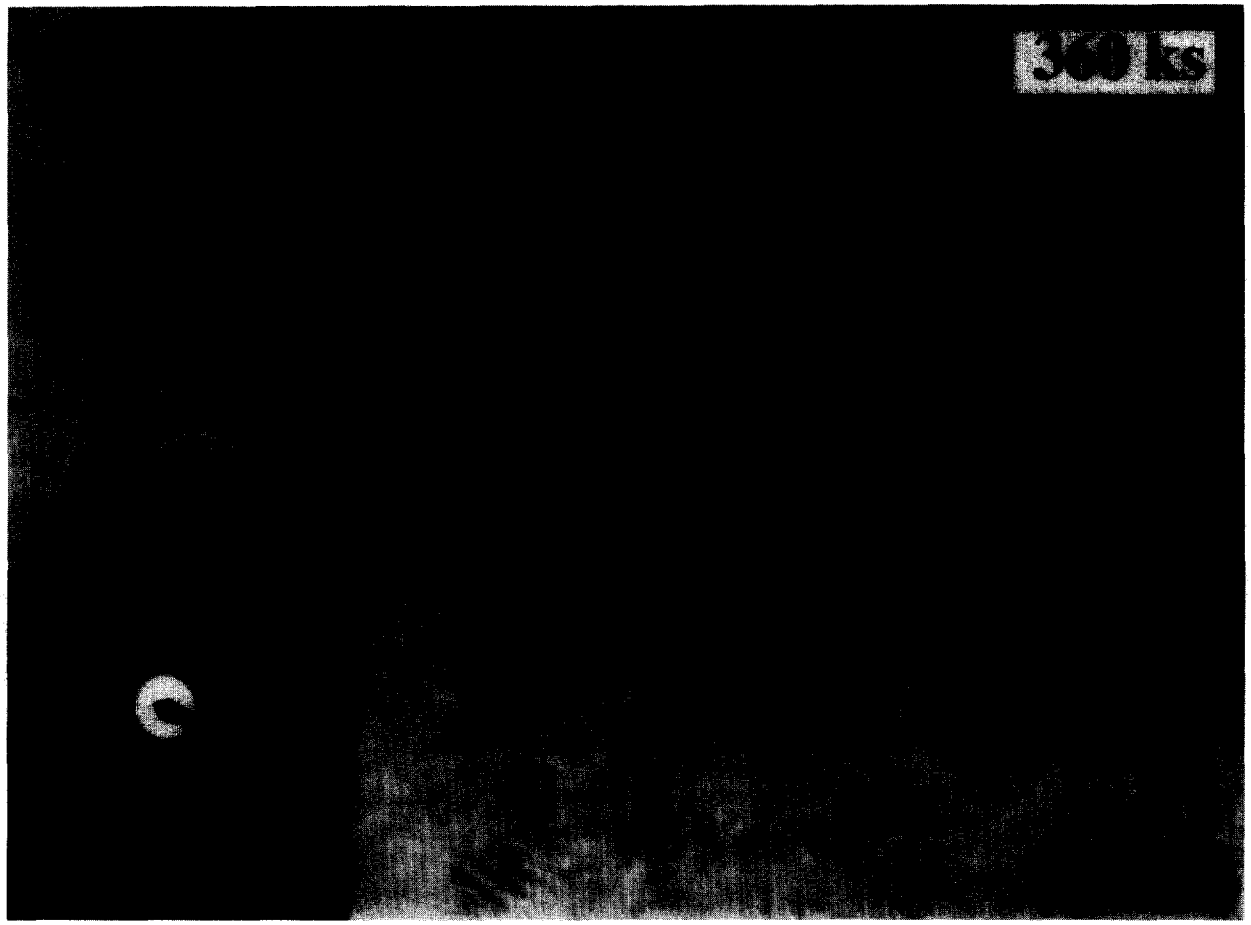

Fig. 5. HRTEM image and SADP taken from a sample of rod-milled $Ti_{50}Al_{50}$ powders after 360 ks of MA time.

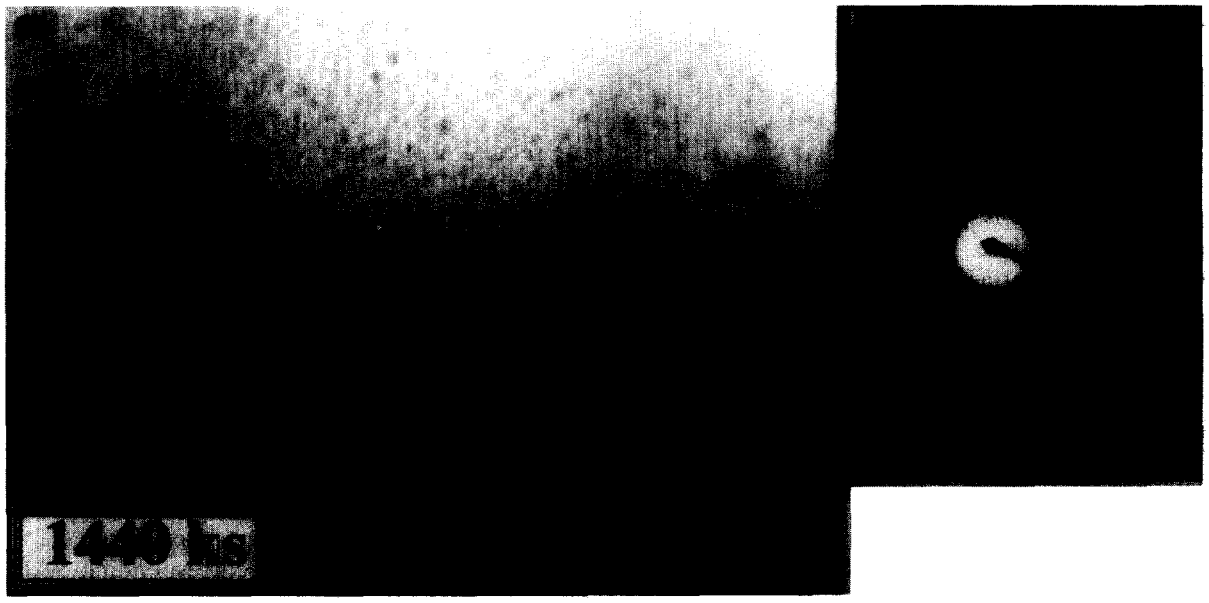

Fig. 6. BFI and SADP taken from a sample of rod-milled $Ti_{50}Al_{50}$ powders at the end of MA time (1440 ks).

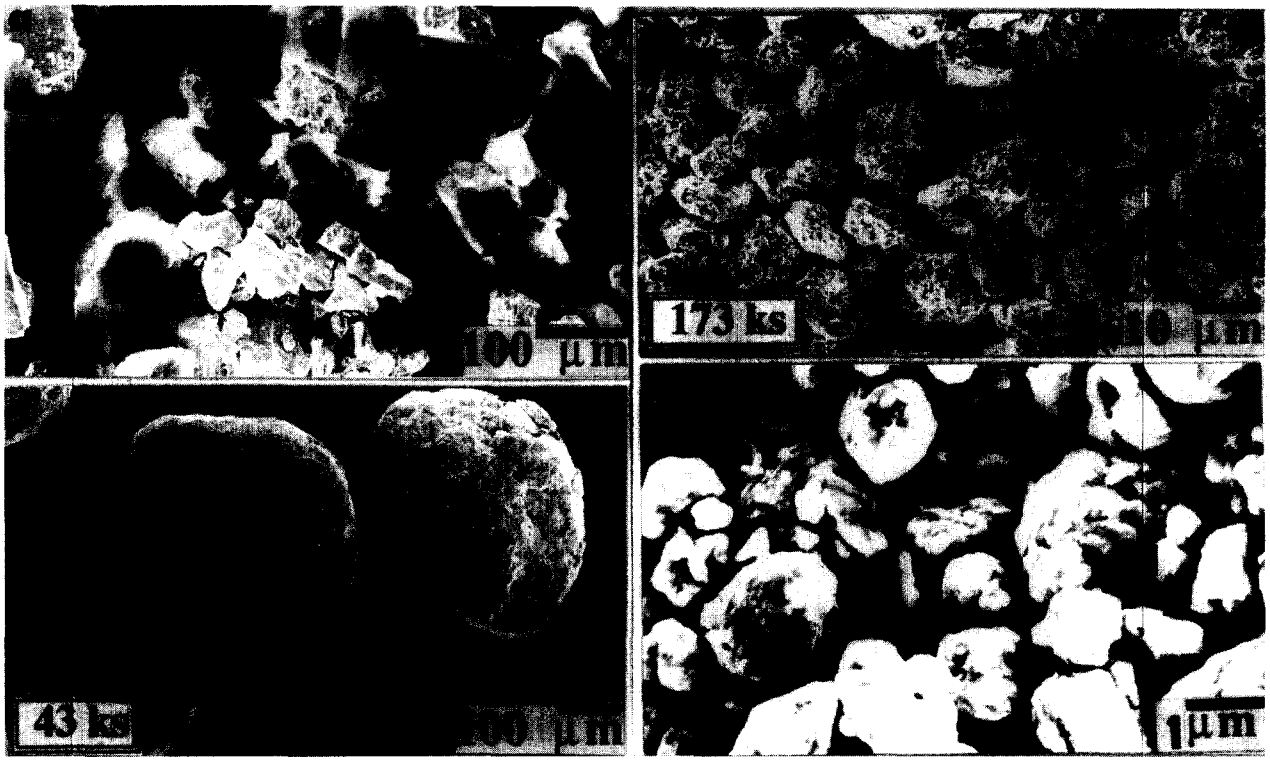

Fig. 7. Detailed SEM micrographs of rod-milled $Ti_{50}Al_{50}$ powders after (a) 0 ks, (b) 43 ks, (c) 173 ks and (d) 1440 ks of MA time.

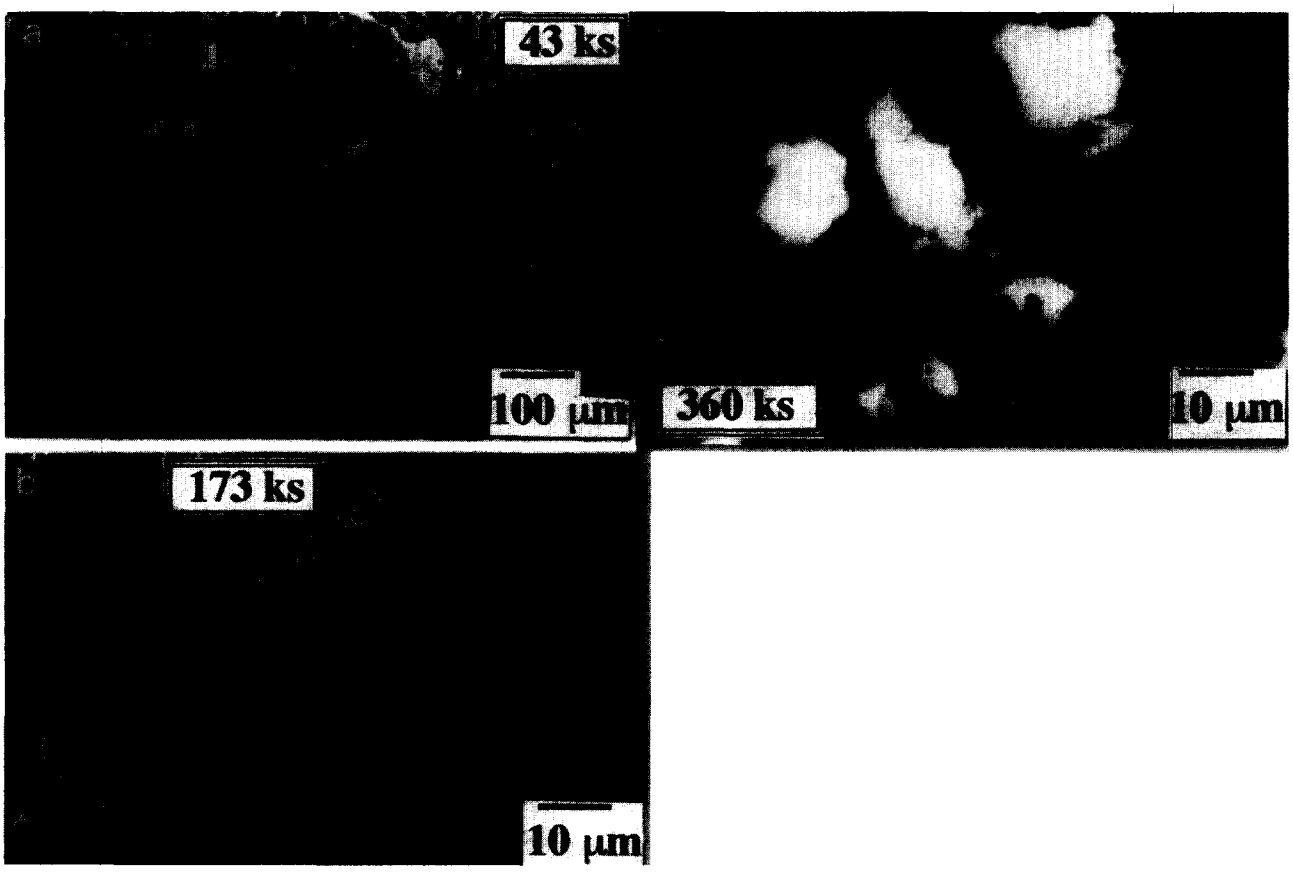

Fig. 8. Optical micrographs of the polished surfaces of rod-milled $Ti_{50}Al_{50}$ powders after (a) 43 ks, (b) 173 ks and (c) 360 ks of MA time.

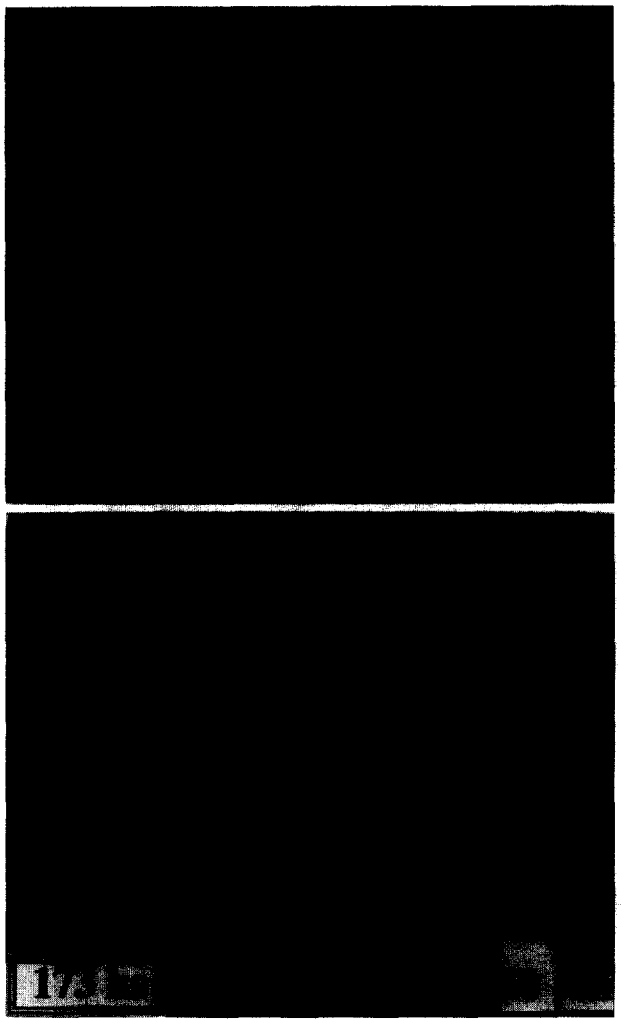

Fig. 9. X-ray dot mapping of (a) Ti and (b) Al elements of rod-milled $Ti_{50}Al_{50}$ powders after 173 ks of MA time.

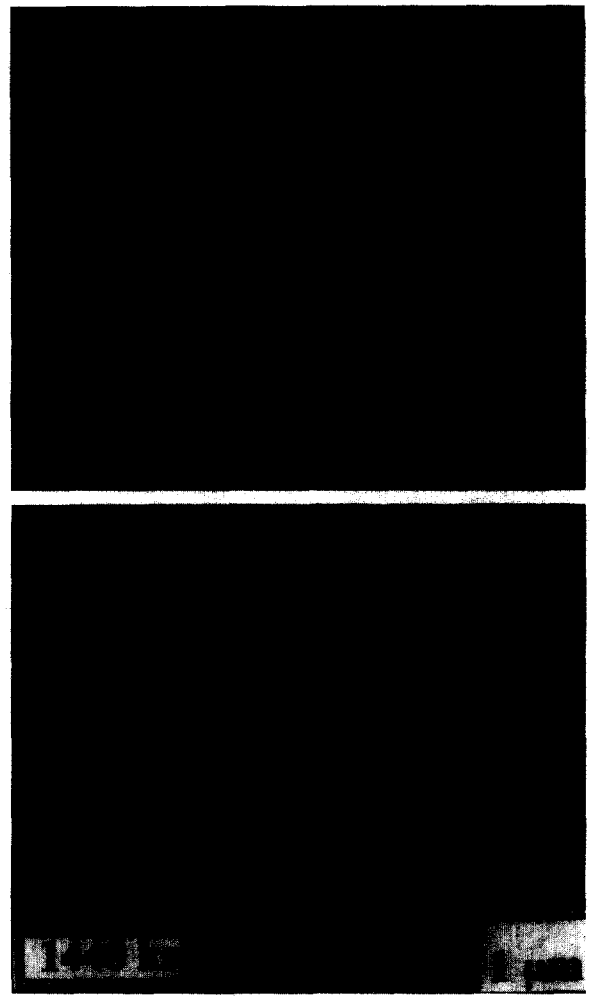

Fig. 10. X-ray dot mapping of (a) Ti and (b) Al elements of rod-milled $Ti_{50}Al_{50}$ powders at the end of MA time (1440 ks).

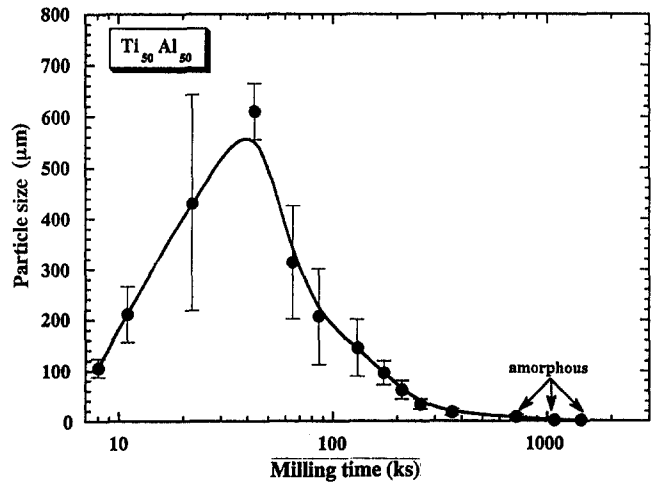

Fig. 11. Influence of the MA time on the particle size distribution of rod-milled $Ti_{50}Al_{50}$ powders.

K (well above the second reaction) are presented in Figs. 14(a), 14(b) and 14(c) respectively. Sample (a) has several nanograins of polycrystalline Ti and Al, and the corresponding SADP from several regions shows spot patterns that are characteristic of diffracting polycrystalline Ti–Al, as displayed in Fig. 14(a). Moreover, the sample has a layered-structure morphology, suggested by the metallographical examination of the polished surface (Fig. 15(a)). Contrary to this, sample (b) taken at 700 K indicates the formation of an amorphous phase, characterized by the fine and featureless image, and clear halo-pattern, as presented in Fig. 14(b). Furthermore, the layered-structure morphology had already disappeared (Fig. 15(b)). In addition, the elemental Ti and Al are distributed uniformly without segregation of the elements, as displayed in Fig. 16. Consequently, it is concluded that the first exothermic peak occurs due to a crystalline-to-amorphous phase transformation conducted by a so-called TASSA reaction. Sample (c) taken at 980 K shows that all regions, without exception, have a cell or grain-like morphology with a sharp ring pattern, as shown in Fig.

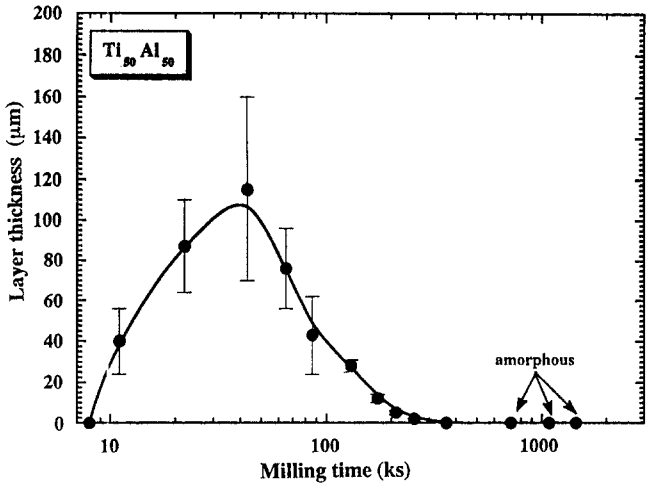

Fig. 12. Effect of the MA time on the layer thickness distribution of rod-milled $Ti_{50}Al_{50}$ powders.

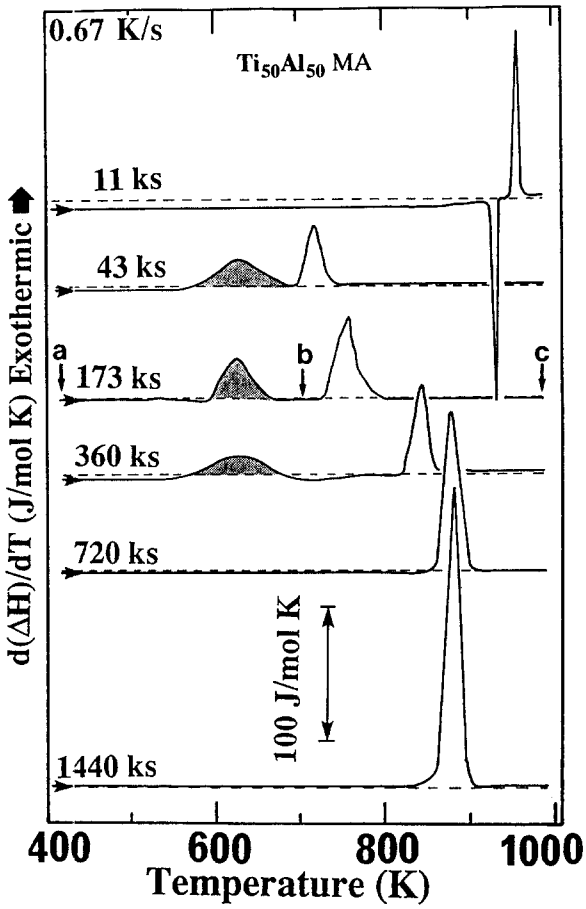

Fig. 13. DSC thermograms associated with the amorphization reactions (the shady low temperature exothermic peaks) and crystallization reactions (the plain high temperature peaks) for rod-milled $Ti_{50}Al_{50}$ powders after selected MA times.

14(c). The Debye–Scherrer ring pattern that can be indexed as polycrystalline TiAl phase (tetragonal structure) is characteristic of an amorphous-to-crystalline phase transformation (crystallization process).

Table 1
Effect of MA time on the activation energy of amorphization E_a for rod-milled $Ti_{50}Al_{50}$ alloy powders

MA time (ks)	E_a (kJ mol^{-1})
22	166
43	167
86	168
173	168

The DSC measurements allow us to obtain the values of the normalized enthalpy of amorphization (heat release of the crystalline-to-amorphous phase transformation) ΔH_a, the amorphization temperature, (temperature of crystalline-to-amorphous phase transformation) T_a, the activation energy of amorphization E_a, the normalized enthalpy of crystallization, (heat release of the amorphous-to-equilibrium crystalline phase transformation), ΔH_x and the crystallization temperature, (temperature of amorphous-to-equilibrium crystalline phase transformation). It is worth noting that T_a does not change with increasing MA time and E_a is substantially independent of the MA time, as shown in Table 1.

In the present study, the term ΔH_a^{TASSA} is used to refer to the heat formation of the amorphous phase (enthalpy of amorphization) via TASSA that has been directly measured from the area under the amorphization peaks.

Fig. 17 presents the correlation between ΔH_a^{TASSA} and the MA time of rod-milled Ti_xAl_{100-x} powders. Also noted is the relationship between the concentration of Ti, x in the milled powders and ΔH_a^{TASSA}. In all compositions, ΔH_a^{TASSA} decreases drastically to approach minimum values and then increases dramatically to zero, as illustrated in Fig. 17. It is worth noting that in the Al-rich side ($x = 33$), the ΔH_a^{TASSA} appears after 65 ks of MA time and approaches a minimum value of -2.3 kJ mol^{-1} after 360 ks of MA. Comparing this with the powders in the Ti-rich side ($x > 33$) the TASSA process in the Al-rich side takes a long time to start (65 ks) and also to end (1080 ks). This is attributed to the fact that the initial composite particles of Ti_xAl_{100-x} in the Al-rich side contain very thick layers of metallic Al so that TASSA cannot be performed between such thick layers [52]. Increasing the milling time leads to refinement of the layers and hence TASSA starts.

In the present work, the term ΔH_a^{MDSSA} is used to refer to the heat formation of an amorphous phase via a MDSSA reaction. However, ΔH_a^{MDASSA} is not a measurable value; it can be estimated only during the final stage of milling (when the amorphization peaks are absent, i.e. $\Delta H_a^{MDASSA} = 0$) using the following relation [53]:

$$\Delta H_{for} = \Delta H_a + \Delta H_x \quad (1)$$

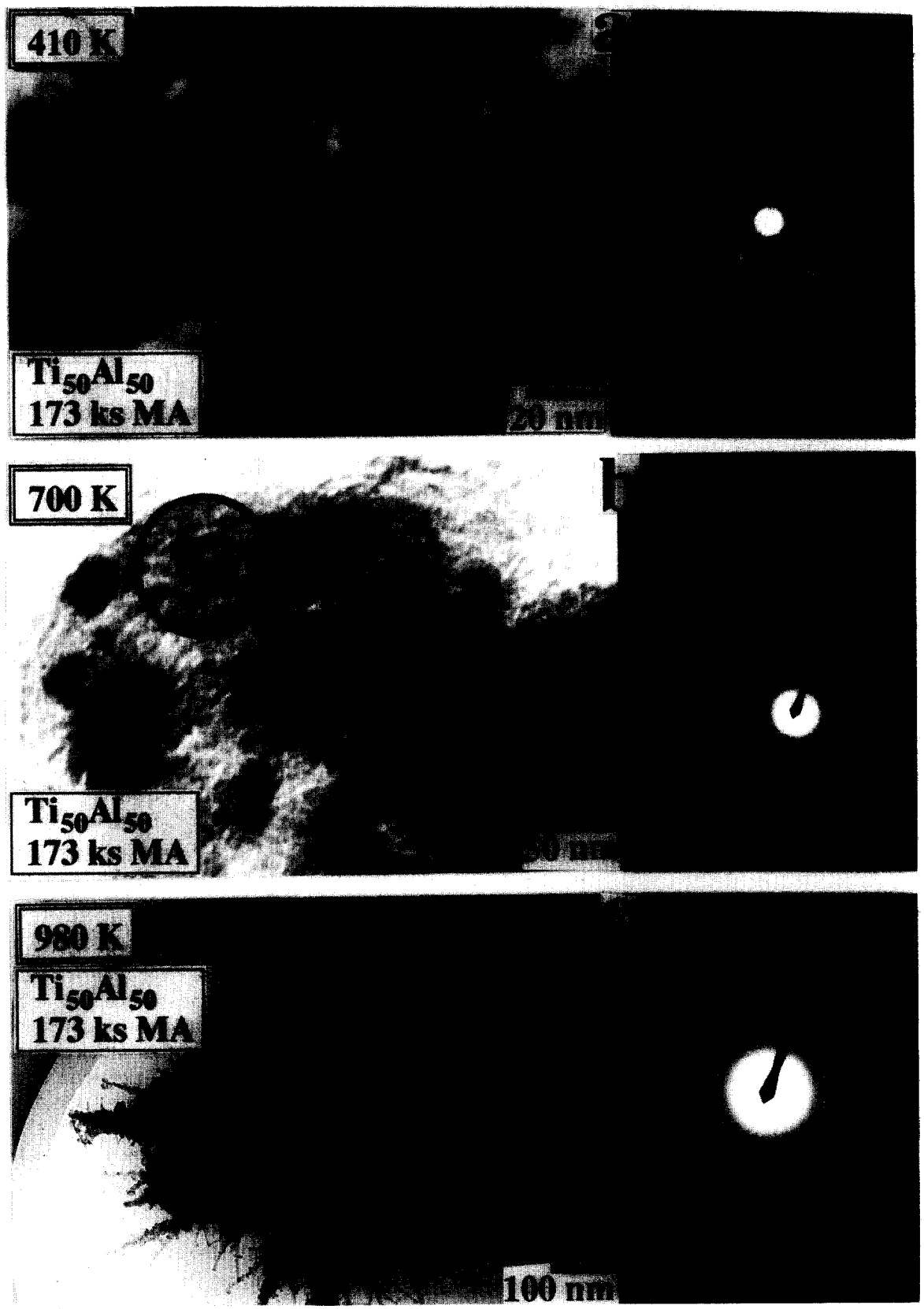

Fig. 14. BFIs and corresponding electron diffraction patterns for 173 ks rod-milled $Ti_{50}Al_{50}$ sample heated to (a) 410 K, (b) 700 K and (c) 980 K in a DSC under argon gas flow.

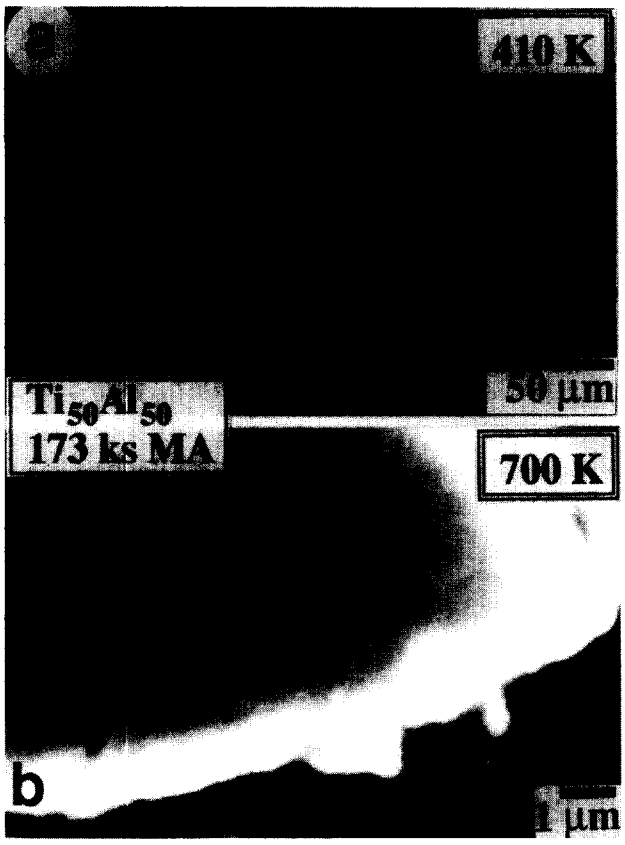

Fig. 15. Optical micrographs of the polished surface for 173 ks rod-milled $Ti_{50}Al_{50}$ powders heated up to (a) 410 K and (b) 700 K. The effect of the annealing temperature on the microstructure of the powder particles is noted.

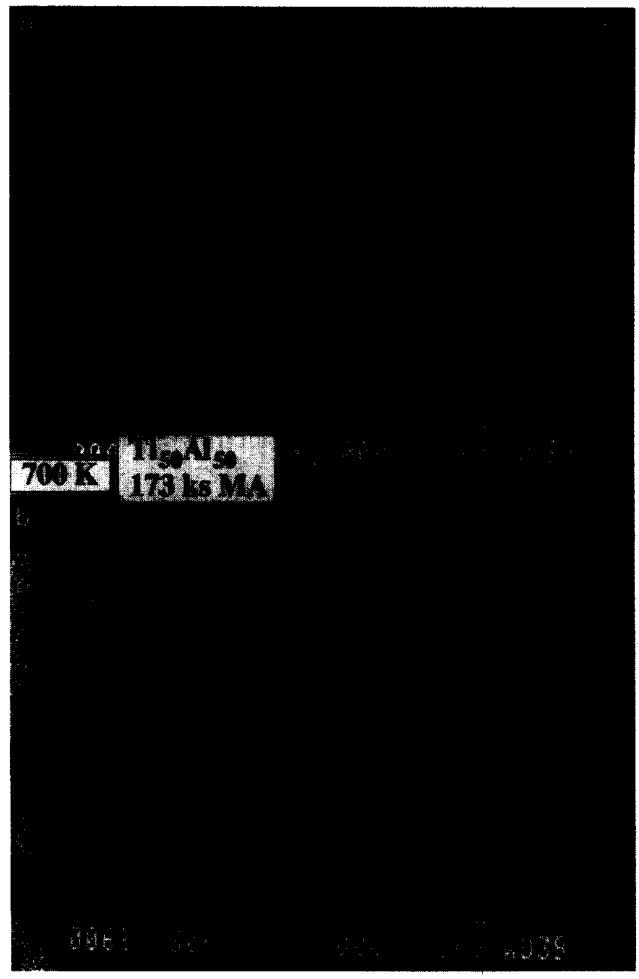

Fig. 16. X-ray dot mapping of (a) Ti and (b) Al elements of rod-milled $Ti_{50}Al_{50}$ powders milled for 173 ks and then heated up to 700 K in a DSC under argon gas flow.

Here, ΔH_{for} is the reported value of the enthalpy of formation for an intermetallic compound at specific concentrations of Ti(x) based on Miedema's model [54], ΔH_a is the total heat of formation of amorphous phases formed by TASSA and MDSSA processes, and the term ΔH_x is considered as the sum of the total enthalpy of crystallization for the amorphous phases caused by the two processes, TASSA and MDSSA. Thus ΔH_a can be given as follows:

$$\Delta H_a = \Delta H_a^{TASSA} + \Delta H_a^{MDSSA} \quad (2)$$

Here, ΔH_a^{TASSA} and ΔH_a^{MDSSA} are the heat of formation of amorphous phases formed by TASSA and MDSSA respectively. Similarly, ΔH_a may also be written as

$$\Delta H_x = \Delta H_x^{TASSA} + \Delta H_x^{MDSSA} \quad (3)$$

Thus, Eq. (1) can be written as

$$\Delta H_{for} = (\Delta H_a^{TASSA} + \Delta H_a^{MDSSA}) + (\Delta H_x^{TASSA} + \Delta H_x^{MDSSA}) \quad (4)$$

During the final stage of milling (the stage in which all the amorphous phase is formed due to the MDSSA

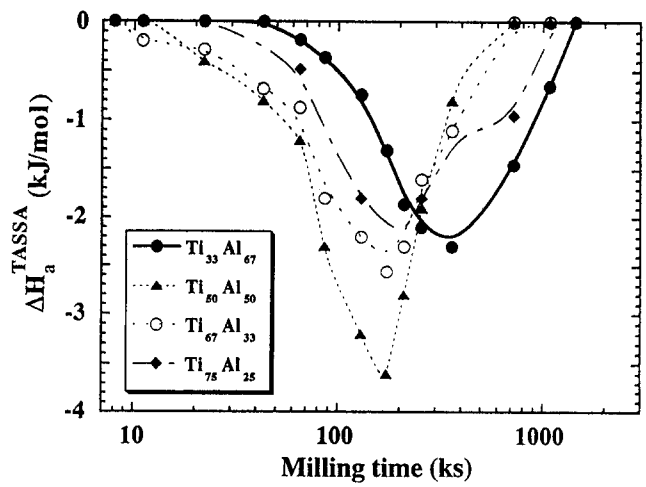

Fig. 17. Dependence of MA time and Ti content on the heat formation of amorphization via TASSA, ΔH_a^{TASSA}, of rod-milled Ti_xAl_{100-x} alloy powders.

process, i.e. when the amorphization reaction peaks are absent, both ΔH_a^{TASSA} and ΔH_x^{TASSA} equal zero. Hence, relation (4) can be rewritten as presented in the following equation:

$$\Delta H_{for} = \Delta H_a^{MDSSA} + \Delta H_x^{MDSSA} \quad (5)$$

The value of ΔH_a^{MDSSA} can then be estimated directly from the following relation:

$$\Delta H_a^{MDSSA} = \Delta H_{for} - \Delta H_x^{MDSSA} \quad (6)$$

In fact, this value is very difficult to estimate at the intermediate stage of milling in which the amorphization peaks are present. At the intermediate stage the measured value of ΔH_x is caused by the crystallization of two amorphous phases resulting from TASSA and MDSSA together.

The correlation between the minimum values of ΔH_a^{TASSA} and ΔH_a^{MDSSA} with the Ti content are presented in Fig. 18. It can be seen that ΔH_a^{MDSSA} is larger than ΔH_a^{TASSA} especially in the Al-rich side.

The amorphization ratios, $\Delta H_a^{MDSSA}/\Delta H_a^{TASSA}$, of Ti_xAl_{100-x} alloy powders are presented in Table 2. In the Al-rich side ($x = 33$) this ratio is about 18, being larger than it is in the Ti-rich side ($x = 75$). This is attributed to the fact that increasing the Al content in the powders leads to the formation of thick layers of Al in the composite particles, then the TASSA process occurs slowly. Thus, the volume fraction of the amorphous phase formed via the TASSA process is small.

3.3.2. Crystallization process

The crystallization characteristics of rod-milled Ti_xAl_{100-x} alloy powders indexed by the crystallization temperature T_x and the enthalpy change of crystallization ΔH_x are presented as a function of the MA time in Figs. 19 and 20 respectively. It can be seen in Fig. 19 that the T_x of Ti_xAl_{100-x} alloys increases monotonically with increasing milling time during the early stage in which the amorphization process occurs only due to

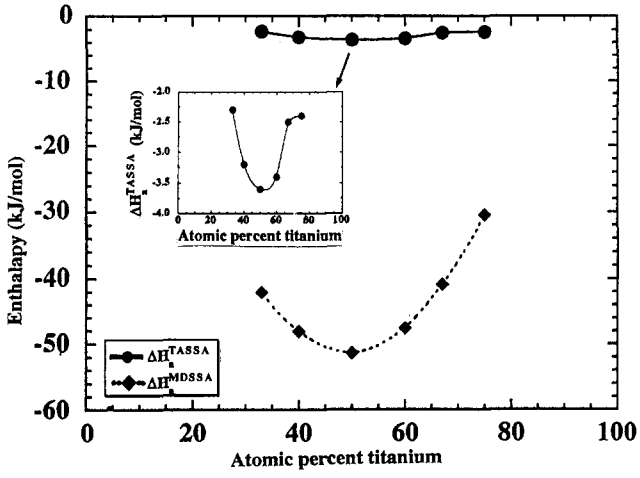

Fig. 18. Correlation between the heat formation (enthalpy change) of amorphization via TASSA, ΔH_a^{TASSA} and MDSSA, ΔH_a^{TASSA}, for rod-milled Ti_xAl_{100-x} alloy powders. The ΔH_a^{TASSA} of Ti_xAl_{100-x} alloy powders is shown inset the figure on another scale.

Table 2
The relative enthalpy of amorphization ratio, $\Delta H_a^{MDSSA}/\Delta H_a^{TASSA}$, for amorphous Ti_xAl_{100-x} alloy powders

Ti content (at. %)	$\frac{\Delta H_a^{MDSSA}}{\Delta H_a^{TASSA}}$
33	18.31
40	15.07
50	14.28
60	14.00
75	12.70

The value of ΔH_a^{MDSSA} was estimated using EQ. (6), whereas ΔH_a^{TASSA} was measured directly using DSC (see the text).

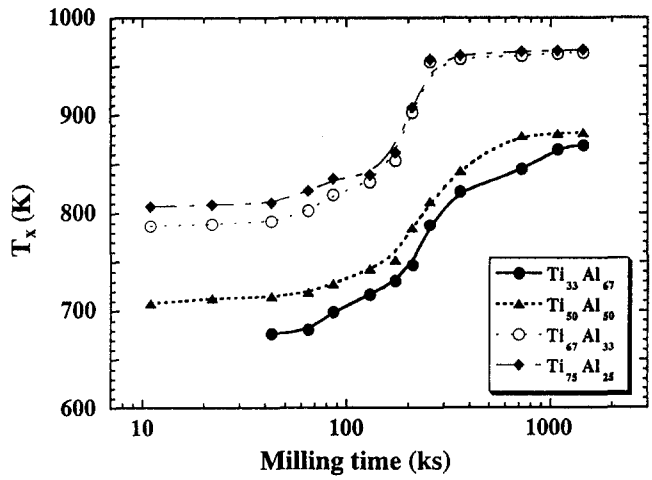

Fig. 19. Effect of the MA time on the crystallization temperature T_x of amorphous Ti_xAl_{100-x} alloy powders.

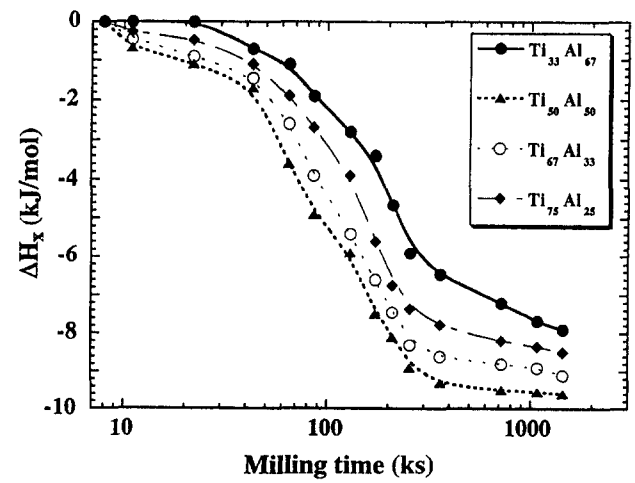

Fig. 20. Effect of the MA time on the enthalpy change of crystallization, ΔH_x, of amorphous Ti_xAl_{100-x} alloy powders.

Table 3
The melting point T_m [55], crystallization temperature T_x, T_x/T_m ratio and the enthalpy of crystallization ΔH_x for amorphous Ti_xAl_{100-x} alloy powders rod-milled for 1440 ks

Ti content (at.%)	T_m (K)	T_x (K)	$\frac{T_x}{T_m}$	ΔH_x (kJ mol^{-1})
33	1693	852	0.503	−7.93
40	1733	869	0.501	−8.97
50	1783	882	0.495	−9.64
60	1863	938	0.503	−9.43
67	1923	964	0.501	−9.18
75	1925	967	0.502	−8.53

the TASSA process. This may suggest a gradual compositional change in the milled powders. It then increases dramatically during the intermediate stage in which the amorphous phases are formed due to the amorphization via TASSA and MDSSA together. These increments in the value of T_x suggest a drastic compositional change of the amorphous phases. During the final stage of milling, however, the amorphous phases of Ti_xAl_{100-x} are formed by the MDSSA process only so that the T_x approaches saturation value even after 1440 ks of MA time.

Further information of the crystallization reactions for Ti_xAl_{100-x} alloy powders are given by ΔH_x and presented in Fig. 20 as a function of the MA time. During the first few kiloseconds of milling the value of ΔH_x decreases monotonically, indicating a gradual increment in the volume fraction of the formed amorphous phases. A rapid increment in the volume fraction of the formed amorphous phase is suggested by the drastic decrease of the ΔH_x during the intermediate stage of milling. Towards the end of the milling process ΔH_x tends to saturated values, suggesting the formation of homogeneous amorphous phases. The ΔH_x for amorphous Ti_xAl_{100-x} alloy powders is presented in Table 3.

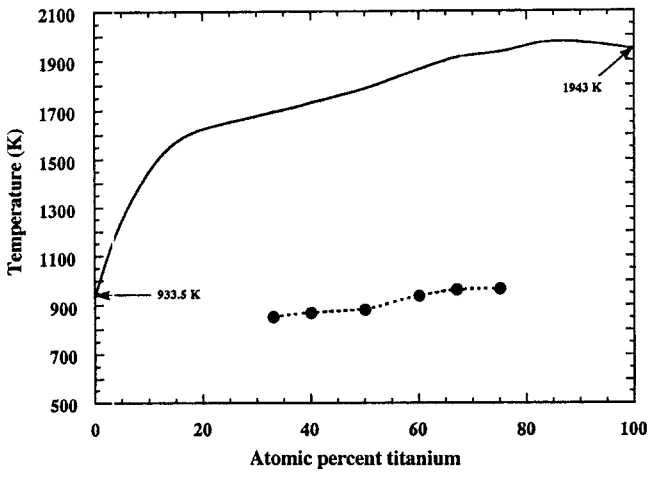

Fig. 21. Correlation between the melting points T_m (solid line) and the crystallization temperatures T_x (dotted line) of Ti_xAl_{100-x} alloy powders.

Fig. 21 illustrates T_x (dotted line) of amorphous Ti_xAl_{100-x} alloy powders after the final stage of milling, i.e. 1440 ks of rod-milling time. In the figure, the melting points T_m of Ti_xAl_{100-x} alloys based on the phase relation diagram [55] are also presented (solid line). It is shown that T_x increases approximately in parallel with T_m. In other words T_x increases with increasing Ti content in the alloy powders. Table 3 shows the T_x/T_m ratio of rod-milled Ti_xAl_{100-x} alloy powders after the final stage of milling, i.e. 1440 ks of rod-milling time. This ratio is about 0.50, being in good agreement with metallic glasses [56–58].

4. Discussion

Amorphous Ti_xAl_{100-x} with wide amorphization range ($33 \leq x \leq 75$) alloy powders have been synthesized by TASSA and/or MDSSA processes, using the rod-milling technique. In the TASSA, heat treatment of composite powder particles containing a well-developed structure of fresh layers of metallic Ti and Al, enhances the solid state diffusion between these thin layers. This leads to a speeding up of the rate of diffusion at the clean Ti–Al boundaries so that the free energy changes drastically from a no stable phase (starting material) to a more stable phase (amorphous). In the MDSSA process the solid state reaction takes place in the same manner as occurs in the TASSA process, except with a lower diffusion rate and a long MA time. This is attributed to the milling temperature that is assumed to be far below that in TASSA (625 K). Thus, the interdiffusion between Ti and Al layers occurs slowly. Although the two processes seem to be the same with different time scales, they produce amorphous alloys which differ widely in thermal stability.

4.1. Amorphization via TASSA; the early stage of milling

This duration of MA time (0 to 43 ks) refers to the first stage of milling in which the amorphization process occurs only due to the TASSA process. During the first few kiloseconds of this stage (0–22 ks), almost all the initial Ti and Al are agglomerated to form powder particles containing many coarse layers of elemental Ti and Al. Further milling (22–43 ks) leads to the formation of composite particles contain numerous narrow layers of Ti and Al in a good arrangement as a result of the shear force generated by the rods. This intensive shear force, accompanied with cold working, create naturally multilayered composite particles typical of sputtered or evaporated diffusion couples before the solid state amorphization

reaction. At this stage, the as-rod-milled powders are a large grain mixture of polycrystalline Ti and Al with sharp grain boundaries. It is worth noting that the formation of the amorphous phase during this stage of milling occurs only due to a TASSA, as shown by DSC. During the DSC measurements of the alloy powders at this stage, two clear separate exothermic peaks appear. The first exothermic reaction occurs at 625 K and the second reaction occurs well above this temperature. The first exothermic peak refers to TASSA in which the free energy of the composite Ti–Al particles decreases from the initial state to the amorphous state. The second exothermic peak occurred due to the crystallization of the amorphous phase formed from the first reaction. The free energy then decreases again from the amorphous state to the equilibrium crystalline state. DSC allows measurement of the enthalpy of amorphization via TASSA ΔH_a^{TASSA} directly.

Once the thickness of Ti and Al layers in the composite particles decreases with increasing MA time, the number of these fresh layers (which become very narrow) increases. The increment of these layers plays a very important role in amorphization via TASSA. ΔH_a^{TASSA} increases drastically with these increasing layers, suggesting a dramatic increase in the volume fraction of amorphous Ti_xAl_{100-x} alloy powders. It is worth noting that when the powder particles have no layers of the starting elements, heating them in the DSC does not lead to the formation of any amorphous phases and ΔH_a^{TASSA} becomes zero.

During the TASSA process, both T_x^{TASSA} and ΔH_x^{TASSA} increase drastically, suggesting a dramatic compositional change and an increase in the volume fraction of the amorphous alloy in the rod-milled powder. The crystallization process at this stage of milling, involves only the crystallizing of the amorphous phase formed by the TASSA process. When the initial materials for rod-milling are intermetallic TiAl powders [50] the amorphization process or so-called MD takes place without compositional change [17]. This is because the final product of the milled powders has the same composition of the starting intermetallic compound powders. It has been already established [59,17] that the amorphization in the MD process requires an increase in the free energy of the compound from the lowest level (most stable phase) to a higher level (less stable phase) [17]. This can be performed in the ball- and/or rod-mills by making the crystalline compound store energy in the form of chemical disorder and point and lattice defects [59], which are typical examples for the MDSSA process. Thus, the DSC curves for MD TiAl powders [51] have shown that the exothermic peaks related to the TASSA process are absent and the process are carried out through a single stage. During all stages of MD process, ΔH_a refers to the heat formation of amorphous TiAl by the MDSSA process only, i.e. ΔH_a^{MDSSA}. This value can be easily estimated at any MD processing time using Eq. (1).

In fact, TASSA is an interesting process in that an amorphous alloy can be formed simply by heating the layered-composite particles to 700 K without further milling. This phenomena has also been shown in mechanically alloyed Ni–Ti [59], Al–Nb [16,18], Al–Ta [21], Al–Zr [20] and Al–Hf [29] binary systems. This process takes place in the same manner of solid state amorphization in artificially metallic multilayer thin films [60,61]. One advantage of the TASSA process is to shorten the milling time; this may lead to formation of amorphous alloy with low contamination contents. However, the amorphous phase formed via the TASSA method is rather heterogeneous, as indicated by the broad crystallization peaks. Moreover, this amorphous phase has a low thermal stability, suggested by the low values of ΔH_x^{TASSA} and T_x^{TASSA}. The thermal stability and homogeneity of the amorphous phase can be improved by further milling times (see the following sections).

4.2. The intermediate stage of milling; the role of amorphization via TASSA and MDSSA processes

In parallel with the TASSA process, a MDSSA begins to take place at the fresh surfaces of Ti–Al layers, with further MA time (43–360 ks). Thus, the amorphization reaction at this stage of milling occurs as a sum of two effects, i.e. TASSA and MDSSA. At the beginning of this stage, the elemental layers of Ti and Al of the composite powders become very thin and have excellent arrangement with numerous interfaces between the diffusion couples. Thus, the value of ΔH_a^{TASSA} decreases dramatically, being larger than ΔH_a^{MDSSA}. In other words, the value of ΔH_x^{TASSA} is larger than ΔH_x^{MDSSA}. Towards the middle of this stage the elemental layers of Ti and Al gradually disappear and the amorphization process occurs mainly due to MDSSA. Thus the values of ΔH_a^{MDSSA} and ΔH_x^{MDSSA} become larger than ΔH_a^{TASSA} and ΔH_x^{TASSA}. Hence, the amorphous phases which formed by way of TASSA plus MDSSA crystallized together through a single broad exothermic peak (overlapped peak), it is very difficult to estimate the values of ΔH_a^{MDSSA}, ΔH_x^{MDSSA} and ΔH_x^{TASSA} during this stage of MA. At the end of this stage (360 ks), the powder particles no longer have a layered-structure morphology and the amorphization process starts to occur only due to MDSSA. Thus, the effect of the TASSA process in the amorphization route can be neglected.

4.3. The final stage of milling; the role of amorphization via the MDSSA process

During this last stage of milling (360–1400 ks) the amorphization process occurs only due to the effect of MDSSA. Thus ΔH_a^{TASSA} and, consequently, ΔH_x^{TASSA} both become negligible. The free energy change of amorphization at this stage can be directly changed from the no stable phase (starting material) to a more stable phase (amorphous). In fact, the amorphous phase formed via the MDSSA process is very homogeneous, and the presence of unprocessed Ti and/or Al atoms in the final product of the alloy powders were not detected. In addition, the alloyed powders possess excellent morphological properties such as homogeneous shape (spherical morphology) with a fine and smooth surface relief with uniform size (less than 1 μm in diameter). During this process, the amorphous Ti_xAl_{100-x} alloy crystallizes through a single sharp exothermic peak, suggesting that the amorphous phase formed is single phase and homogeneous in composition. Owing to the crystallization process, the free energy changes from the amorphous phase to the most stable phase (crystalline). In comparison with TASSA, the amorphization reaction via the MDSSA process occurs fast and much more homogeneously. This is demonstrated by the nearly constant values of ΔH_x^{MDSSA} and ΔH_x^{TASSA}. One disadvantage of the MDSSA process is the long processing time required to change the free energy from the initial state to the amorphous state. This usually causes a rather high contamination of iron and oxygen.

5. Conclusions

This systematic study of the mode of amorphization and crystallization for mechanically alloyed Ti_xAl_{100-x} powders using the rod-milling technique has shown that an amorphous phase could be synthesized in two ways. The first, TASSA, takes place in the mechanically-deformed Ti–Al composite particles by heating the milled powder particles at 700 K in an argon gas atmosphere. In the second process, however, an amorphous phase is formed directly after a long milling time due MDSSA. The amorphization and the crystallization temperatures of amorphous Ti_xAl_{100-x} alloy powders are presented as a function of the milling. Moreover, the heat of amorphization and crystallization have also been investigated.

References

[1] C.C. Koch, O.B. Cavin, C.G. McKamey and J.O. Scarbourgh *Appl Phys. Lett., 43* (1983) 1017.
[2] C. Politis and W.L. Johnson, *J. Appl. Phys., 60* (1986) 1147.
[3] R. Schwarz and C.C. Koch, *Appl. Phys. Lett., 49* (1986) 146.
[4] P.Y. Lee and C.C. Koch, *J. Non-Cryst. Solids, 94* (1987) 88.
[5] E. Hellstern and L. Schultz, *J. Appl. Phys., 63* (1988) 1408.
[6] K. Suzuki, *J. Non-Cryst. Solids, 112* (1989) 23.
[7] E. Gaffet and M. Harmelin, *J. Less-Common Met., 157* (1990) 201.
[8] J.S.C. Jang and C. Koch, *J. Mater. Res., 5* (1990) 498.
[9] M. Sherif El-Eskandarany, F. Itoh, K. Aoki and K. Suzuki, *J. Non-Cryst. Solids, 118* (1990) 729.
[10] R.B. Schwarz, S. Srinivasan and P.B. Desch, *Mater. Sci. Forum, 88–90* (1992) 595.
[11] P. Nash, H. Kim, H. Choo, H. Ardy, S.J. Hwang and A.S. Nash, *Mater. Sci. Forum, 88–90* (1992) 603.
[12] J. Eckert, *Mater. Sci. Forum, 88–90* (1992) 679.
[13] E. Gaffet, N. Malhouroux and M. Abdellaoui, *J. Alloys Comp., 194* (1993) 339.
[14] K.-J. Kim, M. Sherif El-Eskandarany, K. Sumiyama and K. Suzuki, *J. Non-Cryst. Solids, 155* (1993) 165.
[15] M. Sherif El-Eskandarany, K. Aoki and K. Suzuki, *J. Less-Common Met., 167* (1990) 113.
[16] M. Sherif El-Eskandarany, K. Aoki and K. Suzuki, *Scr. Metall., 25* (1991) 1695.
[17] M. Sherif El-Eskandarany, K. Aoki and K. Suzuki, *J. Alloys Comp., 177* (1991) 229.
[18] M. Sherif El-Eskandarany, K. Aoki and K. Suzuki, *J. Appl. Phys., 72* (1992) 2665.
[19] M. Sherif El-Eskandarany, K. Aoki and K. Suzuki, *Mater. Sci. Forum, 88–90* (1992) 81.
[20] M. Sherif El-Eskandarany, K. Aoki and K. Suzuki, *Metall. Trans. A, 23* (1992) 2131.
[21] M. Sherif El-Eskandarany, K. Aoki and K. Suzuki, *J. Appl. Phys., 71* (1992) 2924.
[22] M. Sherif El-Eskandarany, K. Aoki and K. Suzuki, *J. Alloys Comp., 186* (1992) 15.
[23] M. Sherif El-Eskandarany, K. Aoki and K. Suzuki, *J. Non-Cryst. Solids, 150* (1992) 472.
[24] Y. Homma, T. Fukunaga, M. Misawa and K. Suzuki, *Mater. Sci. Forum, 88–90* (1992) 339.
[25] E. Gaffet, F. Faudot and M. Harmelin, *Mater. Sci. Forum, 88–90* (1992) 375.
[26] A.R. Yavari and P.J. Desré, *Mater. Sci. Forum, 88–90* (1992) 43.
[27] D.L. Zhang and T.B. Massalski, *J. Mater. Res., 9* (1994) 53.
[28] E. Ma, *J. Mater. Res., 9* (1994) 592.
[29] M. Sherif El-Eskandarany, K. Aoki, T. Masumoto and K. Suzuki, *J. Alloys Comp., 209* (1994) 71.
[30] T. Tanaka, S. Nasu, K.N. Ishihara and P.H. Shingu, *J. Less-Common Met., 171* (1991) 237.
[31] T. Tanaka, K.N. Ishihara and P.H. Shingu, *Metall. Trans. A, 23* (1992) 2431.
[32] N. Malhouroux-Gaffet and E. Gaffet, *J. Alloys Comp., 198* (1993) 143.
[33] E. Gaffet and N. Malhouroux-Gaffet, *J. Alloys Comp., 205* (1993) 27.
[34] E. Ma, J. Pagán, G. Cranford and M. Atzmon, *J. Mater. Res., 8* (1993) 1836.
[35] M. Sherif El-Eskandarany, K. Sumiyama, K. Aoki and K. Suzuki, *Mater. Sci. Forum, 88–90* (1992) 801.
[36] M. Sherif El-Eskandarany, K. Aoki and K. Suzuki, *Appl. Phys. Lett., 60* (1992) 1562.
[37] M. Sherif El-Eskandarany, K. Sumiyama, K. Aoki and K. Suzuki, *J. Mater. Res., 7* (1992) 888.
[38] K. Aoki, A. Memezawa and T. Masumoto, *J. Mater. Res., 8* (1993) 307.
[39] M. Sherif El-Eskandarany, *J. Alloys Comp., 203* (1994) 117.

[40] M. Sherif El-Eskandarany, K. Sumiyama, K. Aoki, T. Masumoto and K. Suzuki, *J. Mater. Res., 9* (1994) 2891.
[41] K. Aoki, A. Memezawa and T. Masumoto, *J. Mater. Res., 9* (1994) 39.
[42] M. Sherif El-Eskandarany, H.A. Ahmed, K. Sumiyama, and K. Suzuki, *J. Alloys Comp., 218* (1995) 36.
[43] R. Schulz, J.Y. Huot, M.L. Trudeau, L. Dignard, Z.H. Yan, S. Jin, A. Lamarre, E. Ghali and A. van Neste, *J. Mater. Res., 9* (1994) 2998.
[44] M. Sherif El-Eskandarany and H.A. Ahmed, *J. Alloys Comp., 216* (1995) 213.
[45] M. Sherif El-Eskandarany, K. Sumiyama, and K. Suzuki, *J. Mater. Res., 10* (1995) 659.
[46] G.B. Schaffer and P.G. McCormick, *Appl. Phys. Lett., 55* (1989) 45.
[47] G.B. Schaffer and P.G. McCormick, *Met. Trans. A, 21* (1990) 2789.
[48] M. Sherif El-Eskandarany, *Mater. Trans. JIM, 36* (2) (1995) 182.
[49] H.E. Kissinger, *Anal. Chem., 29* (1957) 1702.
[50] M. Sherif El-Eskandarany, K. Sumiyama, K. Aoki and K. Suzuki, *J. Jpn. Soc. Powder Powder Metall., 39* (1992) 836.
[51] M. Sherif El-Eskandarany, K. Aoki and K. Suzuki, *Sci. Rep. Tohoku Univ. A, 39* (1994) 103.
[52] R.B. Schwarz and W.L. Johnson, *Phys. Rev. Lett., 51* (1983) 415.
[53] M.P. Henaff, C. Colinet, A. Pasturel and K.H.J. Buschow, *J. Appl. Phys., 56* (2) (1984) 307.
[54] A.R. Miedema, *J. Less-Common Met., 32* (1973) 117.
[55] T. Massalski, *Binary Alloy Phase Diagrams*, Vol. 1, ASM, 1986, 1st edn., p. 175.
[56] H.A. Davies, *Phys. Chem. Glasses, 17* (1976) 159.
[57] W.L. Johnson, S.J. Poon, J. Durand and P. Duwez, *Phys. Rev. B, 18* (1978) 201.
[58] K.H.J. Buschow, *J. Phys. F:, 14* (1984) 593.
[59] R.B. Schwarz and R.R. Petrich, *J. Less-Common Met., 140* (1988) 171.
[60] M. Van Rossum, M.-A. Nicolet and W.L. Johnson, *Phys. Rev. B, 29* (1984) 5498.
[61] E.J. Cotts, G.C. Wong and W.L. Johnson, *Phys. Rev. B, 37* (1988) 9049.